Mechanical sensors

Enabling Negative Pressure Sensing Through Ferroelectret Device

Yunqi Cao[1*], Hongyang Shi[2**], Xiaobo Tan[2***], and Nelson Sepúlveda[2†]

[1] State Key Laboratory of Industrial Control Technology, College of Control Science, Engineering, Zhejiang University, Hangzhou, Zhejiang 310027, China

[2] Department of Electrical and Computer Engineering, Michigan State University, East Lansing, MI 48824 USA

[*] Member, IEEE

[**] Student Member, IEEE

[***] Fellow, IEEE

[†] Senior Member, IEEE

Manuscript received 22 March 2022; revised 25 June 2022; accepted 30 June 2022. Date of publication 20 July 2022; date of current version 29 July 2022.

Abstract—We report a polypropylene (PP) based ferroelectret device with quasi-piezoelectricity features to measure negative pressures underwater. The device consists of a foam-structured middle layer with giant electric dipoles between two solid PP films. The quasi-piezoelectricity originates from the relative movement between two oppositely charged surfaces under externally applied pressures, which causes a redistribution of surface charges. In this configuration, negative pressure sensing is realized due to the pressure difference caused by the air cavities, which leads to an expansion of the foam and generates an output voltage proportional to the applied pressure. Finite element method (FEM) simulation and experimental validation are both carried out to confirm the mechano-electrical response under negative pressures. Further investigation reveals that the outputs of open-circuit voltage and short-circuit current follow the opposite behavior as that under positive pressures. The proposed tactile sensors can be potentially implemented in wide applications ranging from pneumatic robots to underwater assessment of invasive species.

Index Terms—Mechanical sensors, bidirectional pressure sensing, ferroelectret, negative pressure, self-powered sensors, tactile sensors.

I. INTRODUCTION

Flexible tactile sensors have attracted increasing attention due to their excellent adaptivity to arbitrarily curvilinear surfaces. A variety of emerging applications, such as structural health monitoring [1], tangible user interaction [2], and human–robot interactions [3], are envisioned by the continuing efforts made in this field toward high sensing performances with more accurate real-time tactile information acquisition, higher spatial-resolution pressure mapping, and instantaneous haptic profiles visualization [4]–[6]. Positive pressure (or compression) sensing has been the main focus of research and technological progress since it is the most typical type of pressure in direct human interactions. However, negative pressure (or partial vacuum) sensing is necessary for some applications, such as pipeline leakage detection [10] and monitoring of underwater species [7], [8]. Furthermore, enabling flexible pressure sensors capable of sensing negative pressures is imperative for realizing the ultimate goal of imitating or even augmenting the functionalities of the human sensory system [9].

In triboelectric nanogenerators, microporous structures are often introduced to enhance the change in effective thickness and to modify the dielectric constant under applied pressures [14]. Thus, it is reasonable to expect an electric output due to a change in device capacitance and surface charge density when negative pressure is applied. A similar structure can also be found in polypropylene ferroelectret (PPFE)—which were recently introduced as tactile sensors [15] and energy harvesters [16]—where internal air voids form giant dipole moments, which experiences large deformation under compressive loads contributing to a change in the polarization field that leads to direct mechano-electrical transduction. However, the conversion between the mechanical and electrical energies under negative pressures has not been demonstrated in these devices.

In this letter, a negative pressure sensing mechanism is introduced by using a ferroelectret device. The presented pressure sensor demonstrates quasi-piezoelectricity under negative pressures, which is facilitated by the porous structure of the polypropylene (PP) film. Finite element method (FEM) simulation is used to explain the energy conversion process from mechanical to electrical domains. Experimental characterization of the device further reveals the dependency on input loading amplitudes, loading rates, effective loading area, and the polydimethylsiloxane (PDMS) encapsulation layer thicknesses. The results show that the open-circuit voltage (V_{oc}) increases with the loading amplitude, the short-circuit current (I_{sc}) is proportional to the loading rate, and both electric outputs are positively correlated to the effective loading area. The PDMS thickness has a negligible impact on the device performance. The proposed sensing technology can be useful in several applications, including monitoring underwater invasive species and adhesion force feedback control in pneumatic soft robots.

II. MATERIALS AND WORKING PRINCIPLE

A. Microstructure and Transduction Mechanism

The fabrication of the ferroelectret device starts with a PP film with silicate nanoparticles as stress raisers. When bidirectional in-plane stress is applied, microcracks are formed and propagate along stretching directions, which are expanded into ellipsoid air voids under a high-pressure N_2 environment. The air voids formed in the device have semimajor and semiminor axes in an approximate range of 1–8 μm and 4–40 μm, respectively. The fabrication details as

Corresponding author: Nelson Sepúlveda (e-mail: sepulve6@msu.edu).

Associate Editor: K. Shankar.

Digital Object Identifier 10.1109/LSENS.2022.3192622

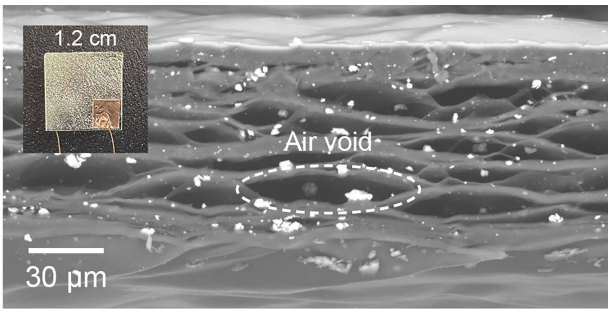

Fig. 1. SEM image of the cross-sectional view of a PP-based ferroelectret device. The inset shows a PPFE sensor.

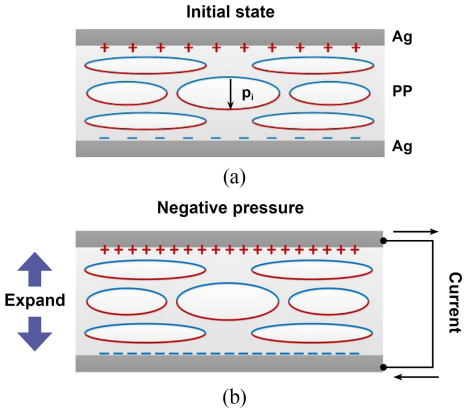

Fig. 2. Schematic illustration of working principle under negative pressure. (a) Surface charge distribution in the initial state. (b) Quasi-piezoelectric effect under negative pressure. The red and blue arc lines/signs represent positive and negative charges, respectively.

well as the quasi-piezoelectricity of the ferroelectret device under positive pressures have been well described in previous work [15]. The device used in this work consists of PPFE film with a thickness of 80 μm. Silver (Ag) thin-film electrodes with a thickness of 500 nm are sputter-coated on both sides of the film. Fig. 1 shows the scanning electron microscope (SEM) image of the cross-sectional view of a PP-based ferroelectret device, where the inset shows the device under test with the side length of 1.2 cm and electrical wires connected to Ag electrodes by using Cu tapes. Each ellipsoidal air void with trapped charges q_i of opposite polarities on top and bottom surfaces can be modeled as a micrometer-sized giant dipole with moment $p_i = q_i l_i$ (also shown in Fig. 2), where l_i is the length of the minor axes, constituting a pressure-sensitive foam structure. In this configuration, the porous region is much more mechanically compliant than the rest of the device, and it occupies approximately 50% of the total volume, thus significantly reducing the elasticity modulus under both compressive and tensile loading.

The quasi-piezoelectricity originates from the change in p_i, which contributes to a change in the polarization field P across the foam thicknesses. The term "quasi" is used because although the device exhibits piezoelectricity, p_i is at micrometer-scale rather than atomic scale and only located in the middle porous region. Therefore, it is essential to investigate the change in P under negative pressures. Fig. 2 presents the schematics of the device's working principle under negative pressure. In the initial state as described in Fig. 2(a), the spontaneous dipole moments p_i caused by the high electric field poling process are well aligned in the same direction through the film thickness. The vector sum of individual moments p_i leads to a polarization field P_0, which

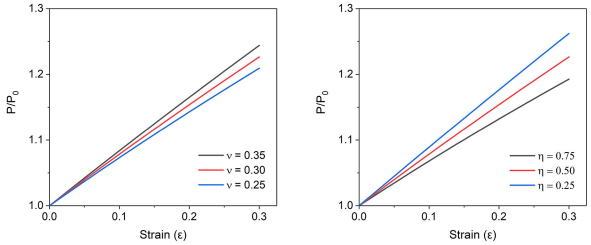

Fig. 3. Analytical simulation of relative polarization field change P/P_0 as a function of ϵ under different (a) Poisson's ratios (ν) and (b) fractions of porous region (η).

gives rise to surface bond charge density (σ_{b1}) in the top and bottom solid PP layers, respectively. Consequently, surface charge density (σ_{b2}) shown as plus and minus signs with opposite polarities is induced at the interface of Ag/PP due to electrostatic induction. As shown in Fig. 2(b), when negative pressure is applied, the elongation of l_i due to film expansion causes a redistribution of P, which can be described as

$$P = \frac{(1+\epsilon)\Sigma_{i=1}^{N} q_i l_i}{[1+(1-2\nu)\epsilon]\,\eta V + (1-\eta)V} \tag{1}$$

where ϵ is the strain of porous region under external pressures, N is the total number of dipole moments, ν is the Poisson's ratio, η is the fraction of porous region, and V is the total volume of the film, assuming a first-order approximation of volumetric change. With the initial polarization expressed as $P_0 = \Sigma_{i=1}^{N} q_i l_i / V$, (1) can be rewritten as

$$P = \frac{1+\epsilon}{1+(1-2\nu)\,\epsilon\eta} P_0. \tag{2}$$

Because the Poisson's ratio ν of a polymer material decreases monotonically with porosity [17], the value for porous PP is lower than the typical value of 0.42 in solid PP films [18]. Fig. 3(a) shows the relative polarization field P/P_0, evaluated with (2) as a function of ϵ under different ν, and with a fixed η of 0.5. It should be noted that, here, the porosity is not the same as η—the former denotes the percentage of void space in the porous region and η is the total volume fraction of this porous region in the film. The influence of η on P/P_0 is also simulated in Fig. 3(b). From Fig. 3, one can see that both ν and η have a certain influence on P. When a negative pressure is applied, we can see that P increases with ϵ, which leads to an enhancement of σ_{b1} and σ_{b2} as shown in Fig. 2(b) and produces an electric signal, measured by the external circuit.

To further examine the transduction mechanism of negative pressure sensing, a 2-D FEM simulation (COMSOL Multiphysics) is carried out. The device used in the simulation has the same cross-sectional structure as illustrated in Fig. 2 with foam dimension of 80 μm in thickness and 300 μm in the side length, and the surface charge density in each air void is 10 mC/m^2. It can be seen in Fig. 4 that positive charges on the top surface and negative charges on the bottom surface increase due to the film expansion, which is consistent with our analytical evaluation. Thus, charges of opposite polarity accumulate at the top of the Ag/PP interfaces, which indicates the voltage difference that would drive a current flow in the external circuit as described in Fig. 2(b).

B. Experimental Setup

The characterization of the quasi-piezoelectric effect under negative pressures was performed by using a soft vacuum suction cup as shown in Fig. 5(a). The sensor was first attached to an acrylic substrate

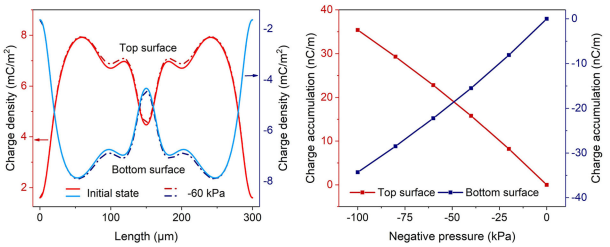

Fig. 4. FEM simulation results of the quasi-piezoelectric effect under negative pressures. (a) Surface charge density on top and bottom surfaces. (b) Charge accumulation at Ag/PP interfaces on top and bottom surfaces.

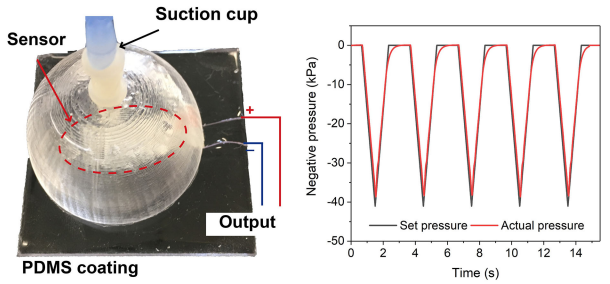

Fig. 5. Experimental methods of device characterization under negative pressures. (a) FENG device was tested in a PDMS-based vacuum suction cup. (b) Waveform of negative pressures generated by the fluidic control board.

by using double-sided tape, then a PDMS encapsulation layer was spin-coated onto the sensor, which provides necessary water resistance for underwater applications. The vacuum pressure in the suction cup is regulated by an open-source fluidic control board [19] using the pulsewidth modulation method. The pressure control apparatus involves a vacuum pump, a solenoid valve, a pressure sensor, and an Arduino microcontroller, which forms a proportional–integral–derivative control system to perform dynamic cyclic loading tests with high repeatability and precision. It should be noted that the diameter of the suction cup is much larger than the sensor dimension so that only negative pressure is applied to the sensor. Fig. 5(b) shows the expected and the actual pressure with triangular waveform generated by the fluidic control board, which are also the mechanical inputs used to characterize the negative pressure response of the sensor. Both V_{oc} and I_{sc} signals were measured by using a Keithley 2450 SourceMeter.

III. RESULTS AND DISCUSSION

The electric output of the sensor under negative pressures is investigated in terms of V_{oc} and I_{sc}. Fig. 6(a) shows time-domain V_{oc} response under cyclic negative pressures with –48 kPa loading amplitude and different loading rates applied on a 0.9 cm × 0.9 cm device. When a negative pressure is applied, σ_{b2} accumulates at the top and bottom Ag/PP interfaces, contributing to a potential difference measured as positive V_{oc} output. Subsequently, when the loading pressure P_{ext} is gradually decreased from its maximum value, σ_{b2} vanishes, and electrons flow back to their original locations, leading to a decrease in V_{oc}. Fig. 6(a) shows that V_{oc} is independent of the pressure loading rate, indicating the linear mechano-electrical coupling effect due to the

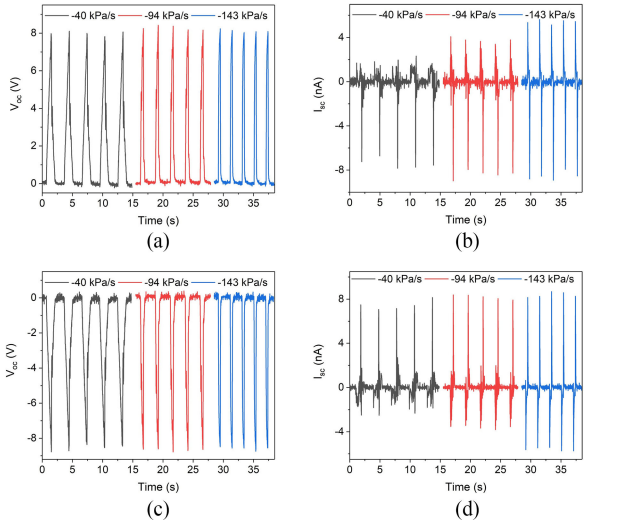

Fig. 6. Waveforms of electric output under negative pressures. Experimental measurements of (a) V_{oc} and (b) I_{sc} under different loading rates. Changing polarity tests of (c) V_{oc} and (d) I_{sc}, when the electric connections are reversed.

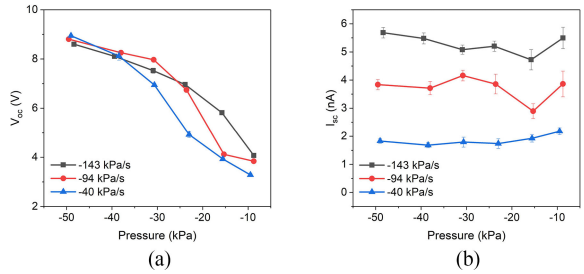

Fig. 7. Dependency of electric output on pressure loading rate. Measurement of (a) V_{oc} and (b) I_{sc} magnitudes as a function of loading pressures under different loading rates.

quasi-piezoelectricity, where V_{oc} is proportional to P_{ext}. When measuring I_{sc} (instead of V_{oc}), the dynamics of σ_{b2} under the negative pressure cycle input shown in Fig. 5(b) causes the current to flow in opposite directions during the pressure loading and unloading stages as can be seen in Fig. 6(b). Since the I_{sc} comes from the displacement current which is proportional to the changing rate of P_{ext}, as $P \propto \partial P_{ext}/\partial t$, the I_{sc} peak-to-peak amplitude increases with pressure loading rate due to the quasi-piezoelectric effect. It should also be noted that the PPFE sensor used in this letter was tested with the opposite polarity compared with our previous work. The quasi-piezoelectricity is further confirmed by the switching polarity tests [20], as shown in Fig. 6(c) and (d); the electric output due to the inverted connection features the same amplitude but opposite polarities compared to the alternative connection.

The loading rate dependency of V_{oc} and I_{sc} is further confirmed in Fig. 7. It can be seen that V_{oc} mainly depends on the pressure amplitude, while I_{sc} is more dependent on the loading rate. The relatively small deviation of the V_{oc} in the –40 kPa/s curve from the other two rates can be observed. When V_{oc} is measured, the internal resistance of the sensor is much lower than the impedance of the measuring instrument, which consumes part of the current during the generation of charge. However, this phenomenon is reduced when the charge generation process is faster. Unlike positive pressures, the generation of negative

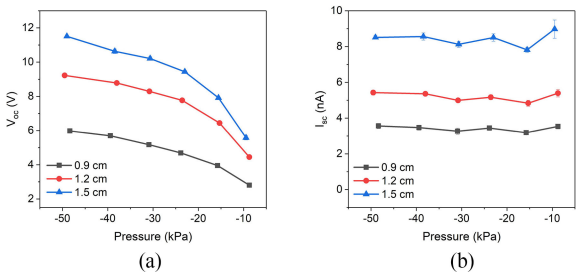

Fig. 8. Dependency of electric output on device surface area. Measurement of (a) V_{oc} and (b) I_{sc} amplitudes as a function of loading pressures under different surface areas.

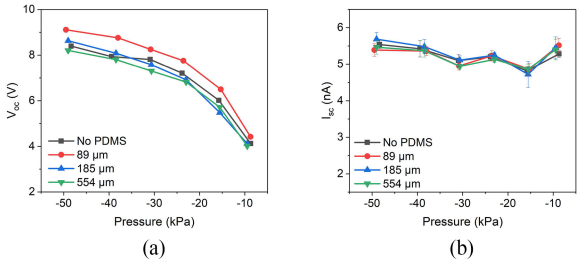

Fig. 9. Characterized relationships between the electric outputs and the encapsulation layer thickness. Measurement of (a) V_{oc} and (b) I_{sc} amplitudes as a function of loading pressures under different encapsulation layer thicknesses.

pressure relies on the use of a mechanical pump, which could transmit high-frequency vibrations to the device through the suction cup, resulting in spiking signals that cause a large standard deviation of I_{sc} especially in the low-pressure range as shown in Fig. 7(b). Given that the quasi-piezoelectricity arises from the accumulation of σ_{b2} under applied pressures, a larger surface area contributes to a larger electric output. To confirm this, three square sensors with different side lengths of 0.9, 1.2, and 1.5 cm were tested, respectively, under various pressures with a constant loading rate of –143 kPa/s. It can be seen from Fig. 8 that both V_{oc} and I_{sc} increase with surface area. In addition, we also evaluated the effect of PDMS encapsulation thickness on the sensor performances, where no obvious change in V_{oc} and I_{sc} is observed for coating thickness up to 554 μm, as shown in Fig. 9. Therefore, the sensor can be integrated with the encapsulation layer for potential underwater detection applications. In addition, because the air cavities are fully embedded inside the solid film, the presented device did not suffer from delamination issues under a negative pressure input.

Potential applications of this sensing technique can be found in feedback control of pneumatic robots which may require a precise measurement of the vacuum force in the suction-based end-effector for vacuum grasping. In addition, the proposed ferroelectret sensors can also be deployed in the underwater environment for *in-situ* detection of invasive sea lampreys, which have a unique suction behavior and causes catastrophic damages to both commercial fishery and ecological systems in the Great Lake region.

IV. CONCLUSION

This letter demonstrates the use of PP film-based devices for measuring negative pressures. The mechano-electrical transduction mechanism is investigated by modeling internal charged voids as macroscale dipole moments and assuming that the deformation only occurs in the porous region. A simple analytical model is proposed to explain the charge generation process, which is further supported by the FEM simulation. The electric output in terms of V_{oc} and I_{sc} are experimentally measured. The results show that the V_{oc} depends mainly on the loading pressure magnitude, while I_{sc} is proportional to the loading rate. Further investigation also reveals the output dependency on the surface area and nondependency on the encapsulation thickness.

V. ACKNOWLEDGMENT

This work was supported in part by the National Natural Science Foundation of China under Grant U21A20519 and in part by the Michigan State University Foundation Strategic Partnership under Grant 16-SPG-Full-3236.

REFERENCES

[1] Y. Cao and N. Sepúlveda, "Design of flexible piezoelectric gyroscope for structural health monitoring," *Appl. Phys. Lett.*, vol. 115, no. 24, 2019, Art. no. 241901.
[2] N. Villar *et al.*, "Project zanzibar: A portable and flexible tangible interaction platform," in *Proc. ACM*, 2018, pp. 1–13.
[3] W. Heng *et al.*, "Fluid-driven soft coboskin for safer human–robot collaboration: Fabrication and adaptation," *Adv. Intell. Syst.*, vol. 3, no. 3, 2021, Art. no. 2000038.
[4] W. Navaraj and R. Dahiya, "Fingerprint-enhanced capacitive-piezoelectric flexible sensing skin to discriminate static and dynamic tactile stimuli," *Adv. Intell. Syst.*, vol. 1, no. 7, 2019, Art. no. 1900051.
[5] L. Nela, J. Tang, Q. Cao, G. Tulevski, and S.-J. Han, "Large-area high-performance flexible pressure sensor with carbon nanotube active matrix for electronic skin," *Nano Lett.*, vol. 18, no. 3, pp. 2054–2059, 2018.
[6] B. Shih *et al.*, "Custom soft robotic gripper sensor skins for haptic object visualization," in *Proc. IEEE Int. Conf. Intell. Robots Syst.*, 2017. pp. 494–501.
[7] H. Shi, C. M. Christopher, Y. Cao, N. Sepúlveda,, and X. Tan,, "Measurement of suction pressure dynamics of sea lampreys, Petromyzon marinus," *PLoS One*, vol. 16, no. 4, 2021, Art. no. e0247884.
[8] I. González-Afanador, H. Shi, C. M. Christopher, X. Tan,, and N. Sepúlveda,, "Invasive sea lamprey detection and characterization using interdigitated electrode (IDE) contact sensor," *IEEE Sens. J.*, vol. 21, no. 24, pp. 27947–27956, Dec. 2021.
[9] H. Wan, J. Zhao, L.-W. Lo, Y. Cao, N. Sepúlveda, and C. Wang, "Multimodal artificial neurological sensory–memory system based on flexible carbon nanotube synaptic transistor," *ACS Nano*, vol. 15, no. 9, pp. 14587–14597, 2021.
[10] M. R. Delgado and O. B. Mendoza, "A comparison between leak location methods based on the negative pressure wave," in *Proc. 14th Int. Conf. Elect. Eng. Comput. Sci. Autom.*, 2017, pp. 1–6.
[11] J. Li, L. Fang, B. Sun, X. Li, and S. H. Kang, "Recent progress in flexible and stretchable piezoresistive sensors and their applications," *J. Electrochem. Soc.*, vol. 167, no. 3, 2020, Art. no. 037561.
[12] C.-M. Lin, L.-Y. Lin, and W. Fang, "Monolithic integration of carbon nanotubes based physical sensors," in *Proc. IEEE 23rd Int. Conf. Micro Electro Mech. Syst.*, 2010, pp. 55–58.
[13] H. Shi *et al.*, "Screen-printed soft capacitive sensors for spatial mapping of both positive and negative pressures," *Adv. Funct. Mater.*, vol. 29, no. 23, 2019, Art. no. 1809116.
[14] X. He *et al.*, "Flexible and transparent triboelectric nanogenerator based on high performance well-ordered porous PDMS dielectric film," *Nano Res.*, vol. 9, no. 12, pp. 3714–3724, 2016.
[15] Y. Cao, J. Figueroa, W. Li, Z. Chen, Z. L. Wang, and N. Sepúlveda, "Understanding the dynamic response in ferroelectret nanogenerators to enable self-powered tactile systems and human-controlled micro-robots," *Nano Energy*, vol. 63, 2019, Art. no. 103852.
[16] Y. Zhang *et al.*, "Ferroelectret materials and devices for energy harvesting applications," *Nano Energy*, vol. 57, pp. 118–140, 2019.
[17] A. D. Drozdov and de J. Claville Christiansen, "The effect of porosity on elastic moduli of polymer foams," *J. Appl. Polym. Sci.*, vol. 137, no. 10, 2020, Art. no. 484494.
[18] G. D. Dean and W. Broughton, "A model for non-linear creep in polypropylene," *Polym. Testing*, vol. 26, no. 8, pp. 1068–1081, 2007.
[19] D. P. Holland *et al.*, "The soft robotics toolkit: Strategies for overcoming obstacles to the wide dissemination of soft-robotic hardware," *IEEE Robot. Autom. Mag.*, vol. 24, no. 1, pp. 57–64, Mar. 2017.
[20] K.-I. Park *et al.*, "Highly-efficient, flexible piezoelectric PZT thin film nanogenerator on plastic substrates," *Adv. Mater.*, vol. 26, no. 16, pp. 2514–2520, 2014.